Eur J Nucl Med Mol Imaging (2015) 42:128–137
DOI 10.1007/s00259-014-2883-7

ORIGINAL ARTICLE

Preclinical evaluation and test–retest studies of [^{18}F]PSS232, a novel radioligand for targeting metabotropic glutamate receptor 5 ($mGlu_5$)

Selena Milicevic Sephton · Adrienne Müller Herde · Linjing Mu · Claudia Keller · Sonja Rüdisühli · Yves Auberson · Roger Schibli · Stefanie D. Krämer · Simon M. Ametamey

Received: 30 May 2014 / Accepted: 28 July 2014 / Published online: 20 August 2014

Abstract
Purpose A novel, ^{18}F-labelled metabotropic glutamate receptor subtype 5 ($mGlu_5$) derivative of [^{11}C]ABP688 ([^{11}C]**1**), [^{18}F]PSS232 ([^{18}F]]**5**), was evaluated in vitro and in vivo for its potential as a PET agent and was used in test–retest reliability studies
Methods The radiosynthesis of [^{18}F]**5** was accomplished via a one-step reaction using a mesylate precursor. In vitro stability was determined in PBS and plasma, and with liver microsomal enzymes. Metabolite studies were performed using rat brain extracts, blood and urine. In vitro autoradiography was performed on horizontal slices of rat brain using **1** and **8**, antagonists for $mGlu_5$ and $mGlu_1$, respectively. Small-animal PET, biodistribution, and test–retest studies were performed in Wistar rats. In vivo, dose-dependent displacement studies were performed using **6** and blocking studies with **7**.
Results [^{18}F]**5** was obtained in decay-corrected maximal radiochemical yield of 37 % with a specific activity of 80 – 400 GBq/μmol. Treatment with rat and human microsomal enzymes in vitro for 60 min resulted in 20 % and 4 % of hydrophilic radiometabolites, respectively. No hydrophilic decomposition products or radiometabolites were found in PBS or plasma. In vitro autoradiography on rat brain slices showed a heterogeneous distribution consistent with the known distribution of $mGlu_5$ with high binding to hippocampal and cortical regions, and negligible radioactivity in the cerebellum. Similar distribution of radioactivity was found in PET images. Under displacement conditions with **6**, reduced [^{18}F]**5** binding was found in all brain regions except the cerebellum. **7** reduced binding in the striatum by 84 % on average. Test–retest studies were reproducible with a variability ranging from 6.8 % to 8.2 %. An extended single-dose toxicity study in Wistar rats showed no compound-related adverse effects.
Conclusion The new $mGlu_5$ radiotracer, [^{18}F]**5**, showed specific and selective in vitro and in vivo properties and is a promising radioligand for PET imaging of $mGlu_5$ in humans.

Keywords $mGlu_5$ · Positron emission tomography · [^{18}F]PSS232 · Test–retest

Selena Milicevic Sephton and Adrienne Müller Herde contributed equally to this work.

S. M. Sephton · A. M. Herde · C. Keller · S. Rüdisühli · R. Schibli · S. D. Krämer · S. M. Ametamey (✉)
Center for Radiopharmaceutical Sciences of ETH, PSI and USZ, Vladimir-Prelog-Weg 4, 8093 Zurich, Switzerland
e-mail: simon.ametamey@pharma.ethz.ch

L. Mu
Department of Nuclear Medicine, University Hospital Zürich, Rämistrasse 100, 8091 Zürich, Switzerland

Y. Auberson
Novartis Institutes for Biomedical Research, Novartis Pharma AG 4002 Basel, Switzerland

Present Address:
S. M. Sephton
Wolfson Brain Imaging Centre, Department of Clinical Neurosciences, Addenbrooke's Hospital, University of Cambridge, Cambridge CB2 0QQ, UK

Introduction

Metabotropic glutamate receptor subtype 5 ($mGlu_5$) is implicated in numerous CNS disorders [1–3] and studies have documented the potential of $mGlu_5$ antagonists as therapeutic targets for anxiety disorders and inflammatory pain [4, 5]. The involvement of $mGlu_5$ has also been shown in other CNS diseases such as schizophrenia [6], depression [7],

neuropathic pain [8, 9] and drug addiction [10]. An important role of $mGlu_5$ has also been established in fragile X syndrome [11], Alzheimer's disease [12, 13] and Parkinson's disease [14, 15]. Furthermore, $mGlu_5$ is believed to participate in the coupling of neuronal activation to cerebral blood flow [16], and upregulation of $mGlu_5$ has been established in patients with amyotrophic lateral sclerosis [17] and focal cortical dysplasia [18].

Carbon-11 labelled (*E*)-3-((6-methylpyridin-2-yl)ethynyl)cyclohex-2-enone *O*-[^{11}C]-methyl oxime ([^{11}C]**1**, [^{11}C] ABP688; Fig. 1) is to date the most widely clinically applied $mGlu_5$ PET radiotracer [19–21, 2, 22, 23]. However, the relatively short physical half-life of ^{11}C (20 min) limits its application to facilities with an on-site cyclotron. Our group aimed to develop a ^{18}F analogue of [^{11}C]**1** that would possess similar or better in vitro and in vivo properties.

Two promising ^{18}F-labelled PET radioligands, namely 3-fluoro-5-((2-([^{18}F]fluoromethyl) thiazol-4-yl)ethynyl)benzonitrile ([^{18}F]**2**, [^{18}F] SP203; Fig. 1) [24, 25] and 3-[^{18}F]fluoro-5-(pyridin-2-ylethynyl)benzonitrile ([^{18}F]**3**, [^{18}F] FPEB; Fig. 1) [26, 27] have also been evaluated in human subjects. However, [^{18}F]**2** exhibited some defluorination, whereas [^{18}F]**3** was produced only in low radiochemical yields. Our group [28–33] evaluated a series of fluorinated compounds and identified (*E*)-3-(pyridin-2-ylethynyl)cyclohex-2-enone *O*-(3-(2-[^{18}F]-fluoroethoxy)propyl) oxime (**5**/[^{18}F]**5**, PSS232 and [^{18}F]PSS232; Fig. 1) as a promising new PET radiotracer. We recently reported [34] on the synthesis and radiosynthesis of **5** and [^{18}F]**5**, which are performed in analogy to the methods previously described for (*E*)-3-(pyridin-2-ylethynyl)cyclohex-2-enone *O*-(2-(3-[^{18}F]-fluoropropoxy)ethyl) oxime (**4**/[^{18}F]**4**, PSS223/[^{18}F] PSS223; Fig. 1) [31]. High binding affinity (1.3 nM) of **5** towards $mGlu_5$ and a favourable experimentally measured log $D_{7.4}$ value of 2 [34] encouraged us to consider **5** as a novel PET radiotracer for imaging $mGlu_5$ density in the brain. We describe here in detail the pharmacological evaluation of [^{18}F]**5** and discuss its in vitro and in vivo properties as well as test–retest performance.

Materials and methods

General

Chemicals and anhydrous solvents were purchased from Aldrich or ABCR (Switzerland). The nonradioactive reference compound and precursor were prepared as previously reported [34]. 2-((3-Methoxyphenyl)ethynyl)-6-methylpyridine (**6**, MMPEP; Fig. 1) and 2-methyl-4-(pyridin-2-ylethynyl)thiazole (**7**, MTEP; Fig. 1) were prepared as previously described [37, 40].

Semipreparative purification of [^{18}F]**5** was performed on a Smartline system with Pump 1000, Manager 5000, Knauer UV detector and GabiStar (Raytest) radiodetector using a reversed-phase column (C18 Phenomenex Gemini, 5 μm, 250 × 10 mm) and eluting with gradient of 5 % to 50 % aqueous MeCN at a flow rate 5 mL/min. Analytical HPLC samples were analysed using an Agilent HPLC 1100 system equipped with a UV multiwavelength detector and a Raytest Gabi star radiation detector using

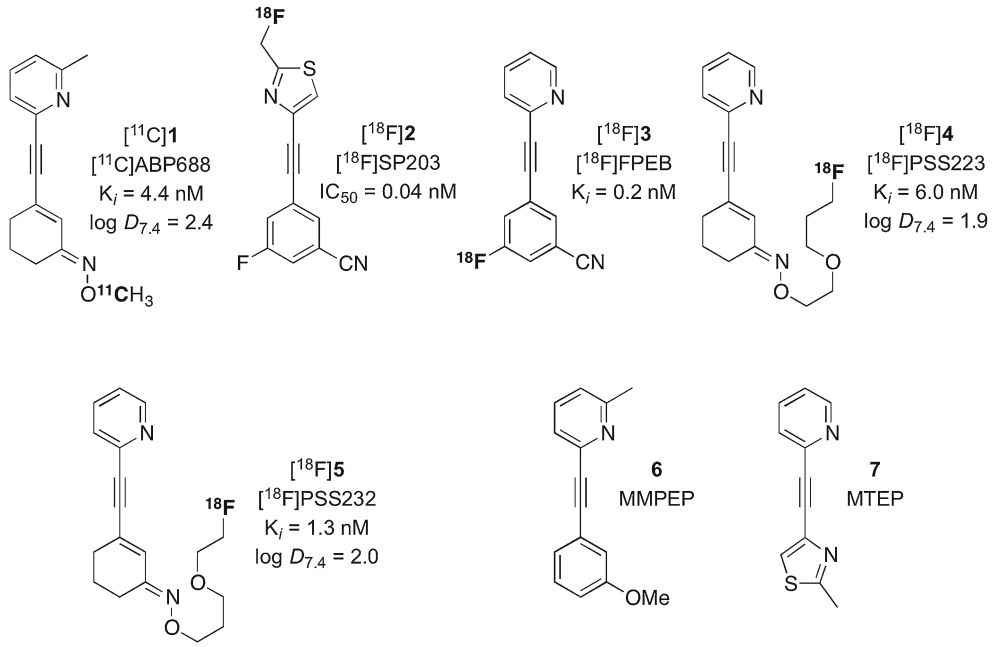

Fig. 1 Chemical structures of various $mGlu_5$ radiotracers and commonly used $mGlu_5$ antagonists

reversed-phase column (ACE 111-0546, C18, 3 μm, 50 × 4.6 mm) and eluting with 45 % aqueous MeCN at a flow rate 1 mL/min.

For all stability studies, samples were analysed by radio-TLC (eluent 2:1 EtOAc/pentane). For biodistribution studies a gamma-counter (Wizard, Perkin-Elmer) was used.

In vitro receptor displacement assay

The binding affinity of **5** to human $mGlu_5$ was determined from three independent displacement experiments with crude membranes (20 μg protein per 200 μL) of human $mGlu_5$-transfected CHO-K1 cells (PerkinElmer, Waltham, MA) and [^{3}H]**1** (2,405 GBq/mmol; AstraZeneca, London, UK) as described previously [34].

Radiosynthesis

The radiosynthesis of [^{18}F]**5** was performed as recently reported [34] but with a slight modification in the formulation. Briefly, [^{18}F]**5** was prepared via aliphatic nucleophilic substitution of the mesylate precursor (2 – 3 mg) with [^{18}F]F^- in the presence of Kryptofix-222® in anhydrous dimethylformamide (0.3 mL) at 95 °C over 10 min. The crude mixture was purified via semipreparative HPLC (retention time 31.0 min). The product was trapped on a C18 cartridge and eluted with EtOH (0.3 mL) in a sterile vial containing 50 % aqueous PEG200 (5 mL) to afford 3 – 12 GBq of the radiolabelled compound. When [^{18}F]**5** was produced in amounts greater than **5** GBq, 25 mg/mL of Na-ascorbate was added as a radical scavenger to avoid observed radiolysis.

Stability studies in PBS and plasma

[^{18}F]**5** (7 – 8 MBq) was incubated in 500 μL phosphate buffer (4 mM KH_2PO_4/Na_2HPO_4, 155 mM NaCl, pH 7.4), or rat or human plasma at 37 °C for up to 3 h. At different time points (0, 30, 60, 100, 130, 180 and 270 min) the enzymatic reactions were stopped by the addition of ice-cold MeCN (140 μL). Plasma samples were centrifuged at 12,000 × *g* for 10 min. The supernatants were filtered and analysed by TLC.

Metabolism studies with liver microsomes

Analogous to a previously described assay [31], [^{18}F]**5** (15 MBq) was preincubated for 5 min at 37 °C with 50 μL NADPH-regenerating system A, 10 μL NADPH-regenerating system B (both BD Biosciences, San Jose, CA), 200 μL TRIS/HCl buffer (75 mM, pH 7.4) and H_2O in a total volume of 975 μL. Rat or human liver microsomes (25 μL; BD Biosciences) were added to a final protein concentration of 0.5 μg/mL. The mixture was incubated at 37 °C at 600 rpm for 1 h. Aliquots of 100 μL were drawn at 0, 5, 10, 20, 40 and 60 min, and immediately quenched with the same volume of ice-cold MeCN. Aliquots were centrifuged at 12,000 × *g* (3 min) and the supernatants were filtered and analysed by TLC. For a negative control (time 0), NADPH-regenerating system and microsomes were replaced by water. Experiments were conducted in triplicate. Note that the enzyme amount and concentration in liver microsomes was different from those in liver in vivo. Metabolism rates were, therefore, different in vitro and in vivo.

In vitro autoradiography

Frozen horizontal slices of the brain (20 μm) from a male Wistar rat (221 g) adsorbed to SuperFrost Plus slides were thawed and preincubated on ice for 10 min in HEPES buffer (30 mM Na-HEPES, 110 mM NaCl, 5 mM KCl, 2.5 mM $CaCl_2 \cdot H_2O$, 1.2 mM $MgCl_2$, pH 7.4) containing 0.1 % bovine serum albumin (BSA; Buchs, Switzerland) and then incubated with 1 nM [^{18}F]**5** alone or together with 100 nM **1** or 100 nM (3,4-Dihydro-2*H*-pyrano[2,3-*b*-]quinolin-7-yl)-(*cis*-4-methoxycyclohexyl)-methanone (**8**, JNJ16259685, Tocris) [35] in HEPES buffer for 45 min at room temperature. The slides were then washed for 5 min in HEPES/0.1 % BSA buffer, 2 × 3 min in HEPES buffer and then briefly dipped in distilled H_2O. Dried slides were exposed to a phosphor imager plate for 30 min, scanned in a BAS5000 reader (Fuji, Tokyo, Japan) and analysed with AIDA v 4.5 software. In vitro autoradiography was repeated five times with horizontal slices from three different Wistar rats.

Animals

Animal care and experiments were conducted in accordance with Swiss Animal Welfare legislation and approved by the Veterinary Office of the Canton Zurich, Switzerland. Male Wistar rats at 5 weeks of age were purchased from Charles River, Sulzfeld, Germany. Unless otherwise stated, for all in vivo experiments animals were anaesthetized with 2 – 3 % isoflurane in oxygen/air.

In vivo metabolite studies

Six rats were injected with about 200 MBq (about 1 nmol) of [^{18}F]**5**. After 20 min the rats were killed by decapitation and blood and urine were collected. Brains were removed and homogenized in 2 mL PBS (pH 7.4) each. Brain homogenates, blood plasma and urine were each mixed with equal volumes of ice-cold MeOH and precipitated proteins were removed by centrifugation (4,800 × *g*, 5 min, 4 °C). Supernatants were analysed by TLC. The lipophilic component consisted of any possible nonpolar radiometabolites and the

parent radiotracer. For the calculations, we assumed equal extraction efficiency for parent tracer and radioligand.

Post-mortem biodistribution studies and dose-dependent displacement

For time-dependent biodistribution studies, 14 – 16 MBq (0.13 – 0.17 nmol) of [^{18}F]**5** was administered by injection into a tail vein. Rats were killed by decapitation at 5, 15, 45 or 95 min after injection (four rats for each time point). For displacement studies, [^{18}F]**5** (14 – 16 MBq, 0.08 – 1.2 nmol) was injected intravenously (i.v.) into anaesthetized rats. After 30 min, 0.1, 0.5 or 1 mg/kg **6** in PEG/H_2O (1:1) or vehicle solution were i.v. injected. This was followed by decapitation 45 min after radiotracer administration (four rats). For blockade experiments, rats were not anaesthetized during i.v. injection of 10 mg/kg **7** in PEG/H_2O (1:1) or vehicle solution, which was immediately followed by injection of [^{18}F]**5** (14 – 16 MBq, 0.09 – 1.3 nmol). Animals were anaesthetized and killed 45 min after injection (four rats).

For all biodistribution studies, organs and brain regions were collected, weighed and measured in a gamma-counter (Wizard 1480; Perkin Elmer). The accumulated radioactivity in the organs is expressed as percentage normalized injected dose per gram of tissue (% normalized ID/g tissue) and for the brain regions as standardized uptake values (SUV) calculated as % ID/g tissue × body weight in grams/100. The displaced fraction of total [^{18}F]**5** binding in the striatum was fitted to the saturation curve function $f(\text{displaced}) = [(f(\text{maximal displaced}) \times \text{dose})/(\text{dose at } f(\text{maximal displaced})/2) + \text{dose}]$.

In vivo PET imaging and displacement study

Anaesthetised rats were positioned on a Vista eXplore PET/CT scanner (Sedecal, Madrid, Spain) and monitored throughout the scan. The activity of i.v. injected [^{18}F]**5** ranged from 25 to 35 MBq (0.1 – 0.18 nmol). Rat body weights were 438 g and 423 g for the displacement and the respective control scans and between 168 g and 256 g for the test–retest study (see below). Dynamic PET scans were acquired in list mode for 90 min. For the displacement study, 1 mg/kg **6** in PEG/H_2O (1:1) was i.v. injected over 50 s starting 40 min after radiotracer injection. We chose this relatively late time point to guarantee tracer equilibration between the involved compartments at the time of MMPEP injection. After the PET acquisition, CT scans were performed for anatomical orientation. PET data were reconstructed using 2-D ordered subsets expectation maximization and analysed with PMOD 3.5 (PMOD Ltd., Zurich, Switzerland). Time–activity curves (TACs) based on the regions of interest (ROIs) defined on the rat MRI T2 template were calculated. Tissue radioactivity values of brain ROIs were decay-corrected and normalized to the injected radioactivity and body weight (SUV).

PET reproducibility and test–retest reliability

Six animals were scanned twice within 7 – 9 days (179.0± 6.2 g at first scan and 243.2±10.8 g at second scan) at the same time of day. PET acquisitions and reconstructions were performed as described above. The area under the TACs (AUC) were calculated from 0 to 4,500 s as the sum of $(A_i/2) \times (t_{i,\,\text{end}} - t_{i,\,\text{start}})$, where A_i is the radioactivity averaged over one brain region and averaged for the time window i, and $t_{i,\,\text{start}}$ and $t_{i,\,\text{end}}$ are the start and end times of the respective time window. Interindividual and intraindividual variability, including relative and absolute differences between AUC of test and retest, intraclass correlation coefficient (ICC), Pearson's correlation coefficient (r), between-subject standard deviation and within-subject standard deviation with the respective coefficients of variation (CV) were calculated according to method of Elmenhorst et al. [36].

Toxicology

The study was performed as an extended single-dose i.v. toxicity study. In this toxicity study, unlabelled **5** was administered once to Wistar rats by i.v. injection into a tail vein. Three groups of ten males and ten females each were treated with 0, 18.86 and 188.6 μg/kg body weight, respectively. The animals were killed 24 h after treatment. The reversibility of treatment-related changes was assessed with five additional animals per sex and group after a treatment-free 14-day recovery period. Mortality, clinical signs, food consumption, body weights, clinical laboratory parameters and organ weights were assessed. A macroscopic examination was performed after the animals had been killed and ten potential target organs were histologically examined.

Statistical analysis

Mean values are given with standard deviations (SD). Results were compared using the uncorrected paired Student's t test. P values <0.05 were considered to indicate statistical significance.

Results

Radiochemical yield and chemical stability

[^{18}F]**5** was typically obtained in a decay-corrected radiochemical yield of 13 – 37 % and specific activity of 80 – 400 GBq/μmol (n=40). [^{18}F]**5** was stable over 270 min in PBS and rat and human plasma.

In vitro and in vivo metabolic stability

In vitro incubation of [^{18}F]**5** with rat and human liver microsomes for 1 h resulted in 20 % and 4 % hydrophilic radiometabolites, respectively (Fig. 2). At 20 min after i.v. administration of [^{18}F]**5** to rats, hydrophilic radiometabolites accounted for 9 % of the total radioactivity in the brain, 46 % in the plasma and 95 % in the urine (Fig. 3).

In vitro autoradiography and selectivity for mGlu5

A heterogeneous binding of [^{18}F]**5** to rat brain slices was observed with the highest radioactivity signals in the hippocampal and cortical regions (Fig. 4). The lowest binding was found in the cerebellum, which is in agreement with the known $mGlu_5$ expression pattern in the brain. Blocking experiments with $mGlu_5$ antagonist **1** showed complete blocking, whereas with **8**, an antagonist for the $mGlu_1$ subtype, no significant changes in radioactivity signals were observed.

The IC_{50} of **5** to human $mGlu_5$ was 1.07±0.66 nM at 4.6±0.6 nM [^{3}H]**1**, similar to the value that we recently determined for rat $mGlu_5$ (1.3±0.1 nM) [34]. An in vitro screening assay using unlabelled **5** showed no significant binding of **5** to adrenergic α-2C, adenosine 3, dopamine D3, histamine H1, melanocortin MC3, muscarinic M1, opiate δ, norepinephrine, dopamine, serotonin, COX-1, COX-2, MoA-A, PDE3, PDE4BD, or PXR receptors (data not shown).

Ex vivo biodistribution studies and dose-dependent displacement

Slow radioactivity washout was observed in all organs during the 95 min after [^{18}F]**5** injection (Fig. 5). For the whole-brain values of 0.31±0.07 % normalized ID/g and 0.07±0.01 % normalized ID/g were measured at 5 min and 95 min after injection, respectively. For displacement studies increasing doses of the $mGlu_5$ antagonist **6** were injected 30 min after injection of [^{18}F]**5**. **6** reduced binding of [^{18}F]**5** in all brain regions except the cerebellum (Fig. 6a). Compared to control (vehicle-treated) animals, the reduction was significant ($P<0.05$) at 1 and 0.5 mg/kg **6** in all brain regions except the cerebellum. At the lowest dose (0.1 mg/kg), the reduction was significant in all brain regions except of the cerebellum, midbrain and thalamus. The fitted **6** dose at half-maximal displacement in the striatum was 0.253 mg/kg and the fitted maximal displacement was 78.5 % of total binding (Fig. 6b). The latter was in perfect agreement with the relative difference of 78.7 % between total binding in the striatum and cerebellum calculated as [(SUVstriatum − SUVcerebellum)/SUVstriatum] × 100. Preadministration of **6** immediately before the tracer was less efficient in blocking than injection 30 min after the tracer (data not shown). We attributed this to the relatively low **6** levels in the brain 40 min after injection [37]. The allosteric $mGlu_5$ antagonist **7** has a biological half-life of >8 h in rats [38], and was therefore injected simultaneously with [^{18}F]**5**. One vehicle-treated rat was excluded as

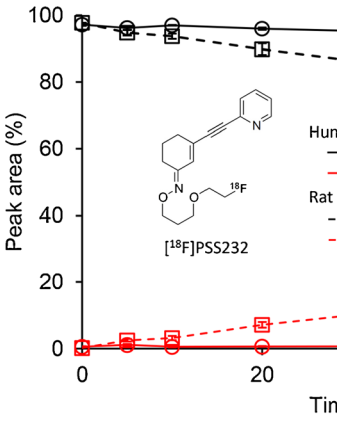

Fig. 2 In vitro stability of [^{18}F]**5** ([^{18}F]PSS232) in the presence of rat and human liver microsomes at equal protein concentrations. The data are presented as mean values and standard deviations of three independent experiments each

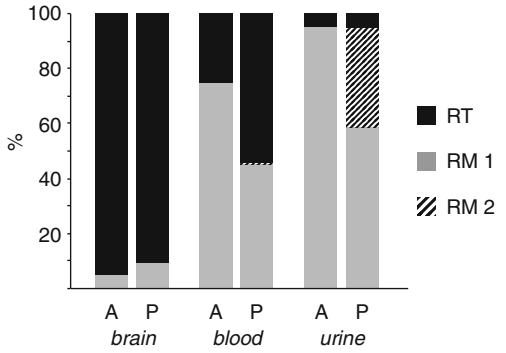

Fig. 3 Radiometabolite studies with rats (n=6) as percentage of intact [^{18}F]**5** and radiometabolites formed at 20 min p.i.: Comparison of intact radiotracer and total radiometabolites in brain, blood and urine of [^{11}C] 1 at 30 min p.i. (A on the graph) and [^{18}F] 5 (P on the graph). *RT* – radiotracer, *RM1-2* – hydrophilic radiometabolites 1 or 2

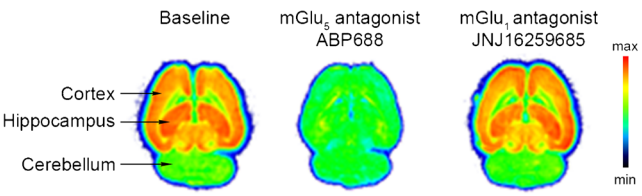

Fig. 4 Representative in vitro [^{18}F]**5** autoradiograms of horizontal slices of rat brain showing heterogeneous radioactivity distribution with the highest binding to the cortex and hippocampus (*red*). The addition of 100 nM $mGlu_5$ antagonist **1** (ABP688) blocked binding, whereas 100 nM $mGlu_1$ antagonist **8** (JNJ16259685) did not affect [^{18}F]**5** binding. *Note*: Striatal regions known to show high $mGlu_5$ expression are not in the plane of these rat brain slices. The slices correspond to the plates designated as PW116, bregma −3.10 mm (Paxinos and Watson, The Rat Brain Atlas, 1998 edition)

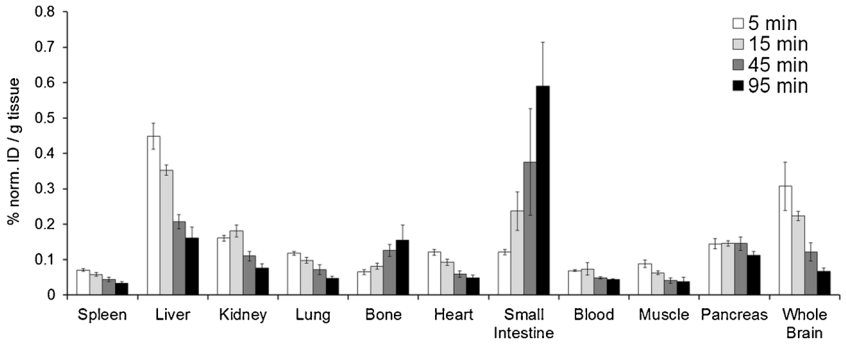

Fig. 5 Post-mortem biodistribution studies of [^{18}F]**5** in rats at 5, 15, 45 and 95 min after injection (four rats for each time point)

the calculated uptake values were unrealistically high. $mGlu_5$ antagonist **7** reduced binding in the striatum by 84.1 % on average (Fig. 6a). Reduction was significant in all brain regions ($P<0.01$) except the cerebellum ($P>0.05$) with an average reduction of 16.2 %.

Small-animal PET imaging

Figure 7a shows representative PET images of [^{18}F]**5** superimposed on MR images of a rat brain. The highest uptake of radioactivity was seen in $mGlu_5$-rich brain regions such as the striatum, hippocampus and cortex, in agreement with in vitro autoradiography and ex vivo biodistribution studies. A negligible amount of radioactivity was observed in the cerebellum.Figure 7b shows TACs of rat brain regions from a [^{18}F]**5** dynamic PET scan. To verify the specificity of [^{18}F]**5** binding in vivo, **6** (1 mg/kg) was administered i.v. 40 min after radiotracer injection. Shortly after **6** administration radioactivity values had decreased in all brain regions to the level in the cerebellum (Fig. 7c). Maximal displacement was reached within 10 – 15 min after injection and remained until the end of the scan, confirming maximal displacement efficiency in the ex vivo biodistribution experiments where MMPEP was injected 15 min before dissection.

PET reproducibility and test–retest reliability

[^{18}F]**5** accumulation in the cerebellum was low and hardly displaceable. The cerebellum was therefore used as the reference region in the following analyses. Accumulation of radioactivity is expressed as the AUC (0 – 4,500 s) ratio between the ROI and the cerebellum. Values >1 indicate specific accumulation. Average AUC ratios ranged from 1.3 in the midbrain to 2.5 in the striatum (Table 1). AUC ratio determinations were reproducible with a variability ranging from 6.8 % to 8.2 %. The mean relative difference for the ROIs between test and retest was −7.1 %. The ICCs were between 0.22 and 0.53 and r values for individual brain regions were between 0.63 and 0.94. The between-subject CV (%CV >5.0) exceeded the within-subject CV (%CV <4.9) in all ROIs.Figure 8 shows the correlation between test and retest AUC ratios in individual animals and brain regions. AUCs in the retest group were lower than the values in the test group for all brain regions, resulting in an overall slope of <1 with r= 0.982.

Toxicology

In the single-dose study in Wistar rats administration of **5** at a dose up to 1,000-fold the intended human dose did not cause

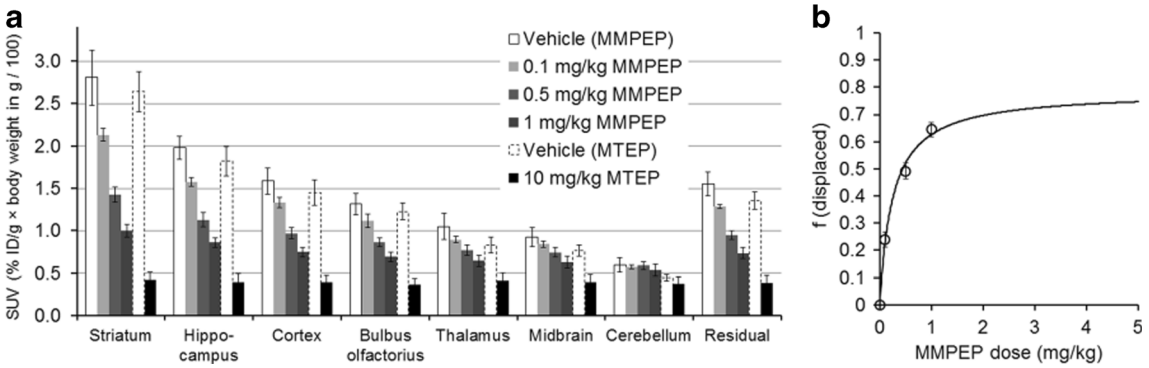

Fig. 6 Post-mortem biodistribution study of [^{18}F]**5** in rat brain. **a** Dose-dependent displacement by **6** (MMPEP) or blocking with **7** (MTEP; four rats for each condition, except three rats for MTEP vehicle). **b** Displaced fraction in the striatum as a function of **6** (MMPEP) dose

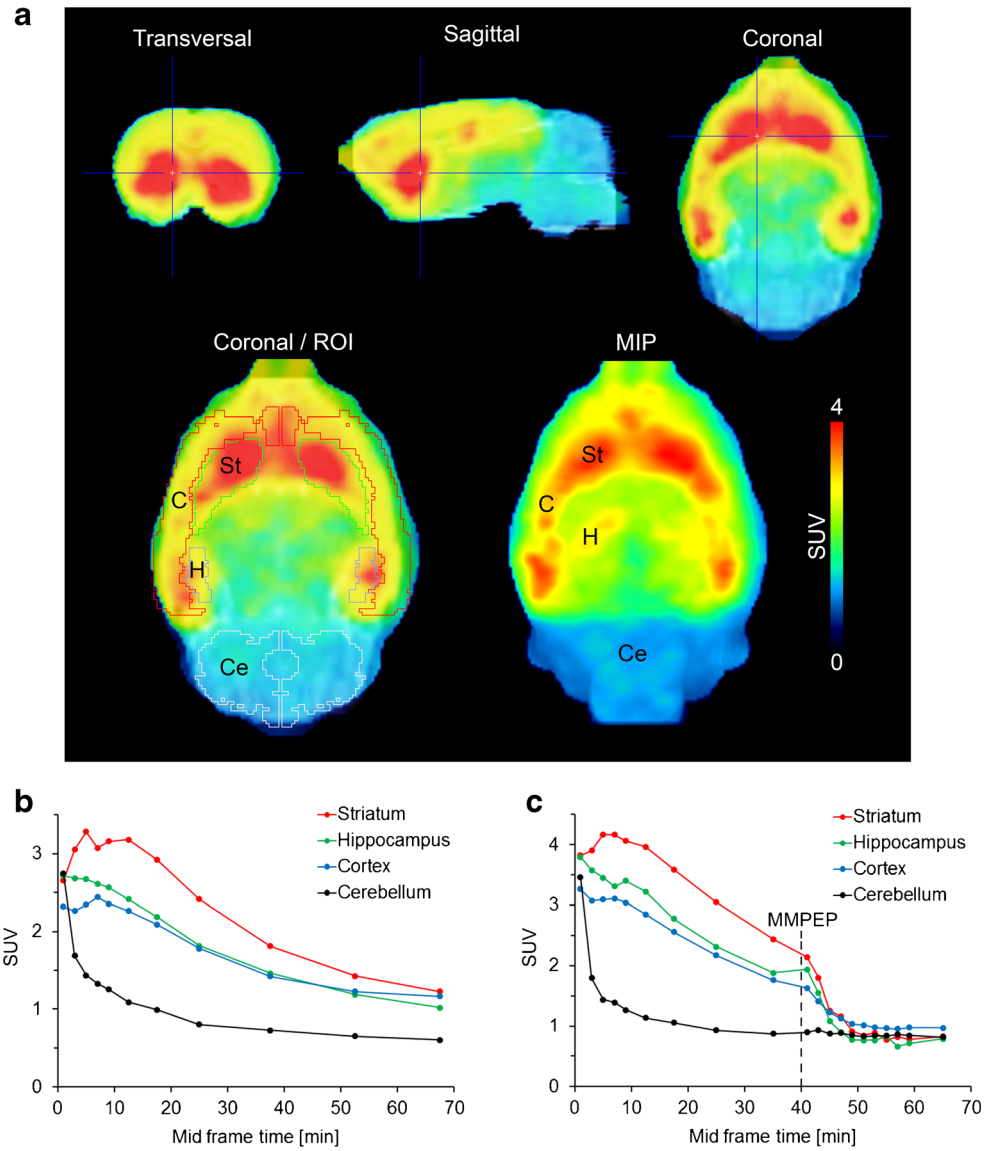

Fig. 7 **a** PET images of [^{18}F]**5** (averaged for 2 – 30 min after injection of 35 MBq) in a rat brain. The PET images (*coloured*) are superimposed on an MRI T2 template (*grey*). The *top row* shows a transverse, sagittal and coronal plane with the striatum in the cross hairs. The *bottom row* shows brain ROIs for quantitative analysis and a maximal intensity projection (*St* striatum, *C* cortex, *H* hippocampus, *Ce* cerebellum). **b** TACs for [^{18}F]**5** in different brain regions. **c** [^{18}F]**5**-TACs at displacement with 1 mg/kg **6** (MMPEP) 40 min after radiotracer injection

any signs of toxicity, as assessed by mortality, clinical signs, body weight, food consumption, necropsy, clinical biochemistry, and macroscopic and microscopic observations.

Discussion

The derivatization of the **1** structural manifold to incorporate ^{18}F has resulted in dramatic changes as demonstrated by the poor signal-to-noise ratio with 2-methyl-4-(pyridin-2-ylethynyl)thiazole ([^{18}F] **9**, [^{18}F]FDEGPECO) [33] and the rapid defluorination of [^{18}F]**4** in vivo [31]. A facile enzymatic cleavage of the C–F bond at the end of the side chain is a possible reason for the rapid defluorination observed in **4** [31]. Interestingly, switching the oxygen atom located between the ethylene and the fluoropropyl moieties by one CH_2 unit to the right in the side chain resulted in the metabolically more stable **5** (Fig. 1), which also retained high binding affinity for $mGlu_5$ [34]. The in vitro selectivity profile of **5** was also high given that no significant interaction with other prominent CNS receptors was observed. Furthermore, the selectivity of [^{18}F]**5** for $mGlu_5$ over $mGlu_1$ was confirmed by in vitro autoradiography (Fig. 4). Compared with other clinically tested ^{18}F $mGlu_5$ PET radiotracers ([^{18}F]**2** and [^{18}F]**3**), [^{18}F]**5** has the advantage that it has a robust radiosynthetic protocol which allows efficient and practical routine daily production. [^{18}F]**5** was obtained in a maximum chemical yield of 37 % (decay-corrected) and high specific activity.

We initially determined the in vitro stability of our new tracer in PBS and rat and human plasma, and with liver microsomal enzymes. While **5** was stable in PBS, and in rat

Table 1 Test–retest reliability of AUC ratios (means±SD from six rats) for [^{18}F]**5** ([^{18}F]PSS232)

Region	AUC ratio		% Relative difference	% Variability	ICC	Pearson's *r*	Between-subject SD (% CV)	Within-subject SD (% CV)
	Test	Retest						
Striatum	2.59±0.14	2.43±0.19	−6.0±4.8	6.9±3.9	0.53	0.78	0.179 (7.1)	0.103 (4.1)
Hippocampus	2.13±0.06	1.96±0.11	−7.8±3.9	8.2±4.2	0.25	0.73	0.122 (6.0)	0.100 (4.9)
Cortex	2.13±0.08	1.97±0.08	−7.6±3.1	7.9±3.4	0.22	0.63	0.114 (5.6)	0.095 (4.6)
Thalamus	1.62±0.07	1.50±0.06	−7.2±1.7	7.5±1.8	0.30	0.90	0.086 (5.5)	0.066 (4.2)
Midbrain	1.38±0.05	1.29±0.05	−6.5±1.2	6.8±1.3	0.31	0.94	0.066 (5.0)	0.050 (3.8)
Whole brain	1.82±0.06	1.70±0.07	−7.6±1.4	7.0±1.6	0.28	0.92	0.087 (5.0)	0.068 (3.9)

AUC ratio is the ratio between the AUC of the ROI and the AUC of a 52-mm^3 sphere in the centre of the cerebellum (to avoid spillover effects)

and human plasma, radiometabolites were formed in the presence of rat microsomes. With human liver microsomes only 4 % of hydrophilic radiometabolites was observed. Considering species differences [39, 31], as shown through in vitro experiments, no significant defluorination is expected in humans. Based on our TLC analysis, we cannot exclude the formation of one or more lipophilic radiometabolites with a Rf (ratio to front) value similar to that of [^{18}F]**5**. Thus, the lipophilic component consisted of the total amount of parent radiotracer and any potential lipophilic radiometabolite(s), which could have contributed to the nondisplaceable radioactivity.

PET images confirmed that **5** successfully crossed the blood–brain barrier as expected from the log $D_{7.4}$ of **2**. In comparison to other $mGlu_5$ radiotracers such as [^{18}F]**3** [40] which shows the highest activity accumulation 30 min after injection, [^{18}F]**5** has a faster initial uptake and a steeper washout curve slope with a maximum at 5 min after injection in the brain. In the periphery, the highest accumulation of radioactivity was found in the liver, suggesting hepatobiliary excretion. Coadministration of **6** resulted in a dose-dependent displacement of [^{18}F]**5** in all brain regions except the cerebellum. TACs from PET decreased after injection of **6** to the level in the cerebellum. The perfect agreement between the fitted maximal displacement by **6** in the striatum and the difference between the striatum and cerebellum radioactivity under baseline conditions indicates that the cerebellum is free of receptor and, therefore, provides an ideal reference region for kinetic modelling. While maximal blockade was not reached with the highest dose of **6** (1 mg/kg) administered 10 min before the animals were killed, injection of **7** (10 mg/kg) immediately before tracer administration reached the extrapolated maximal displacement. **7** may therefore be better suited to in vivo blocking studies than **6**.

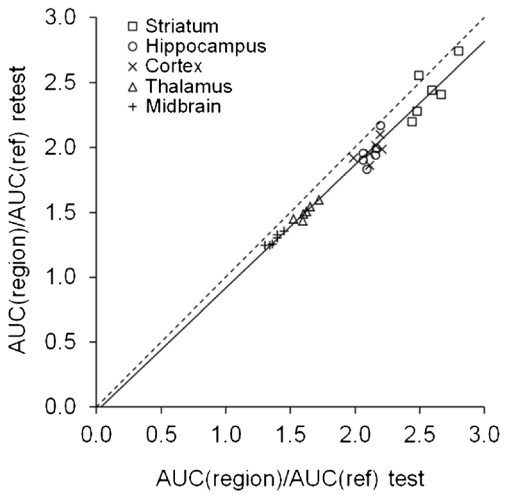

Fig. 8 Scatter plot of test AUC ratios versus retest AUC ratios from PET scans in individual animals (*AUC(ref)* AUC of a 52-mm^3 sphere in the centre of the cerebellum (from six rats)

We examined the robustness of noninvasive receptor density quantification using [^{18}F]**5** PET as well as the test–retest reproducibility. For these analyses, we aimed for a simple, model-independent and assumption-free quantification method with high reproducibility. Comparing the AUCs of the ROI and the reference region fulfilled these requirements for [^{18}F]**5** and allowed any bias introduced by the assumption of a particular kinetic model or by a parameter required for model-dependent analysis without prior evaluation to be avoided. The relatively low interindividual variability of the AUC ratios within one measurement group allows quantitative preclinical PET with [^{18}F]**5** with relatively small group sizes. All AUC ratios from the retest group were lower than from the test group, but were reproducible with a variability of 6.8 % to 8.2 %. Our reliability parameters for [^{18}F]**5** are in good agreement with the previously published measurements for [^{11}C]**1** by Elmenhorst et al. [36]. We are currently

characterizing the kinetics of [^{18}F]**5**, including in more detail the AUC ratio method applied in this study.

Conclusion

[^{18}F]**5** is a new fluorinated derivative which can be reliably prepared in high radiochemical yield and high specific radioactivity. The new radioligand was demonstrated to readily cross the blood–brain barrier and to specifically and selectively bind to $mGlu_5$-rich regions in the rat brain. Noninvasive quantification of [^{18}F]**5** imaging is reproducible and reliable, and no signs of toxicity were observed in an extended single-dose study in Wistar rats. The overall preclinical profile of [^{18}F]**5** indicates that it is a promising fluorinated PET radioligand for imaging $mGlu_5$ receptors in humans. Work is in progress to validate the utility of [^{18}F]**5** in a clinical research programme.

Acknowledgments The authors thank Aretussa Apladas and Martin Hungerbühler for technical support in the PET laboratory, Daniel Bieri, Dr. Lukas O. Dialer and Dr. Cindy R. Fischer for assistance with the biodistribution experiments, Stjepko Cermak (Institute Rudjer Boskovic, Zagreb, Croatia) for assistance with the test–retest study, and Susanne Geistlich for the toxicity studies. Dr. Thomas Nauser and Martina Dragic are acknowledged for support in the radiochemistry lab as well as Dominique Leutwiler with the microsome stability assays.

Conflicts of interest None.

References

1. DeLorenzo C, Kumar JSD, Mann JJ, Parsey RV. In vivo variation in metabotropic glutamate receptor subtype 5 binding using positron emission tomography and 11C-ABP688. J Cereb Blood Flow Metab. 2011;31(11):2169–80.
2. Deschwanden A, Karolewicz B, Feyissa AM, Treyer V, Ametamey SM, Johayem A, et al. Reduced metabotropic glutamate receptor 5 density in major depression determined by 11C-ABP688 PET and postmortem study. Am J Psychiatry. 2011;168(7):727–34.
3. Lüscher C, Huber KM. Group 1 mGluR-dependent synaptic long-term depression: mechanisms and implications for circuitry and disease. Neuron. 2010;65:445–59.
4. Ritzen A, Mathiesen JM, Thomsen C. Molecular pharmacology and therapeutic prospects of metabotropic glutamate receptor allosteric modulators. Basic Clin Pharmacol. 2005;97(4):202–13.
5. Spooren W, Ballard T, Gasparini F, Amalric M, Mutel V, Schreiber R. Insight into the function of group I and group II metabotropic glutamate (mGlu) receptors: behavioral characterization and implications for the treatment of CNS disorders. Behav Pharmacol. 2003;14:257–77.
6. Ohnuma T, Augood SJ, Arai H, McKenna PJ, Emson PC. Expression of the human excitatory amino acid transporter 2 and metabotropic glutamate receptors 3 and 5 in the prefrontal cortex from normal individuals and patients with schizophrenia. Mol Brain Res. 1998;56(1-2):207–17.
7. Pilc A, Klodzinska A, Branski P, Nowak G, Palucha A, Szewczyk B, et al. Multiple MPEP administrations evoke anxiolytic- and antidepressant-like effects in rats. Neuropharmacology. 2002;43(2):181–7.
8. Cosford ND, Tehrani L, Roppe J, Schweiger E, Smith ND, Anderson J, et al. 3-[(2-Methyl-1,3-thiazol-4-yl)ethynyl]-pyridine: a potent and highly selective metabotropic glutamate subtype 5 receptor antagonist with anxiolytic activity. J Med Chem. 2003;46(2):204–6.
9. Gasparini F, Lingenhohl K, Stoehr N, Flor PJ, Heinrich M, Vranesic I, et al. 2-Methyl-6-(phenylethynyl)-pyridine (MPEP), a potent, selective and systemically active mGluR5 receptor antagonist. Neuropharmacology. 1999;38(10):1493–503.
10. Chiamulera C, Epping-Jordan MP, Zocchi A, Marcon C, Cottiny CC, Tacconi S, et al. Reinforcing and locomotor stimulant effects of cocaine are absent in mGluR5 null mutant mice. Nat Neurosci. 2001;4(9):873–4.
11. Todd PK, Mack KJ, Malter JS. The fragile X mental retardation protein is required for type-I metabotropic glutamate receptor-dependent translation of PSD-95. Proc Natl Acad Sci U S A. 2003;100(24):14374–8.
12. Bruno V, Ksiazek I, Battaglia G, Lukic S, Leonhardt T, Sauer D, et al. Selective blockade of metabotropic glutamate receptor subtype 5 is neuroprotective. Neuropharmacology. 2000;39(12):2223–30.
13. Wang Q, Walsh DM, Rowan MJ, Selkoe DJ, Anwyl R. Block of long-term potentiation by naturally secreted and synthetic amyloid beta-peptide in hippocampal slices is mediated via activation of the kinases c-Jun N-terminal kinase, cyclin-dependent kinase 5 and p38 mitogen-activated protein kinase as well as metabotropic glutamate receptor type 5. J Neurosci. 2004;24(13):3370–8.
14. Ossowska K, Konieczny J, Wardas J, Pietraszek M, Kuter K, Wolfarth S, et al. An influence of ligands of metabotropic glutamate receptor subtypes on Parkinsonian-like symptoms and the striatopallidal pathway in rats. Amino Acids. 2007;32(2):179–88.
15. Rouse ST, Marino MJ, Bradley SR, Awad H, Wittmann M, Conn PJ. Distribution and roles of metabotropic glutamate receptors in the basal ganglia motor circuit: implications for treatment of Parkinson's disease and related disorders. Pharmacol Ther. 2000;88(3):427–35.
16. Zonta M, Angulo MC, Gobbo S, Rosengarten B, Hossmann KA, Pozzan T, et al. Neuron-to-astrocyte signaling is central to the dynamic control of brain microcirculation. Nat Neurosci. 2003;6(1):43–50.
17. Aronica E, Catania MV, Geurts J, Yankaya B, Troost D. Immunohistochemical localization of group I and II metabotropic glutamate receptors in control and amyotropic lateral sclerosis human spinal cord: upregulation in reactive astrocytes. Neuroscience. 2001;105(2):509–20.
18. Aronica E, Gorter JA, Jansen GH, van Veelen CW, van Rijen PC, Ramkema M, et al. Expression and cell distribution of group I and II metabotropic glutamate receptor subtypes in Taylor-type focal cortical dysplasia. Epilepsia. 2003;44(6):785–95.
19. Ametamey SM, Kessler LJ, Honer M, Wyss MT, Buck A, Hintermann S, et al. Radiosynthesis and preclinical evaluation of 11C-ABP688 as a probe for imaging the metabotropic glutamate receptor subtype 5. J Nucl Med. 2006;47(4):698–705.
20. Ametamey SM, Treyer V, Streffer J, Wyss MT, Schmidt M, Blagoev M, et al. Human PET studies of metabotropic glutamate receptor subtype 5 with 11C-ABP688. J Nucl Med. 2007;48(2):247–52.
21. Burger C, Deschwanden A, Ametamey S, Johayem A, Mancosu B, Wyss M, et al. Evaluation of bolus/infusion protocol for 11C-ABP688, a PET tracer for mGluR5. Nucl Med Bio. 2010;37(7):845–51.
22. Treyer V, Streffer J, Wyss MT, Bettio A, Ametamey SM, Fischer U, et al. Evaluation of the metabotropic glutamate receptor subtype 5 using PET and 11C-ABP688: assessment of methods. J Nucl Med. 2007;48(7):1207–15.
23. Wyss MT, Ametamey SM, Valerie T, Andrea B, Blagoev M, Kessler LJ, et al. Quantitative evaluation of 11C-ABP688 as PET ligand for

the measurement of the metabotropic glutamate receptor subtype 5 using autoradiographic studies and beta-scintillator. Neuroimage. 2007;35(3):1086–92.
24. Shetty HU, Zoghbi SS, Simeon FG, Liow JS, Brown AK, Kannan P, et al. Radiodefluorination of 3-fluoro-5-(2-(2-[18F](fluoromethyl)-thiazol-4-yl)ethynyl)benzonitrile ([18F]SP203), a radioligand for imaging brain metabotropic glutamate subtype-5 receptors with positron emission tomography, occurs by glutathionylation in rat brain. J Pharmacol Exp Ther. 2008;327(3):727–35.
25. Simeon FG, Brown AK, Zoghbi SS, Patterson VM, Innis RB, Pike VW. Synthesis and simple 18F-labeling of 3-fluoro-5-(2-(2-(fluoromethyl)thiazol-4-yl)ethynyl)benzonitrile as a high affinity radioligand for imaging monkey brain metabotropic glutamate subtype-5 receptors with positron emission tomography. J Med Chem. 2007;50(14):3256–66.
26. Barret O, Tamagnan G, Batis J, Jennings D, Zubal G, Russell D, et al. Quantitation of glutamate mGluR5 receptor with 18F-FPEB PET in humans. J Nucl Med. 2010;51 Suppl 2:215.
27. Wong DF, Waterhouse R, Kuwabara H, Kim J, Brasic JR, Chamroonrat W, et al. 18F-FPEB, a PET radiopharmaceutical for quantifying metabotropic glutamate 5 receptors: a first-in-human study of radiochemical safety, biokinetics, and radiation dosimetry. J Nucl Med. 2013;54(3):388–96.
28. Baumann CA, Mu L, Wertli N, Kramer SD, Honer M, Schubiger PA, et al. Syntheses and pharmacological charazterization of novel thiazole derivatives as potential mGluR5 PET ligands. Bioorg Med Chem. 2010;18(16):6044–54.
29. Honer M, Stoffel A, Kessler LJ, Schubiger PA, Ametamey SM. Radiolabeling and in vitro and in vivo evaluation of [18F]-FE-DABP688 as a PET radioligand for the metabotropic glutamate receptor subtype 5. Nucl Med Biol. 2007;34(8):973–80.
30. Lucatelli C, Honer M, Salazar JF, Ross TL, Schubiger PA, Ametamey SM. Synthesis, radiolabeling, in vitro and in vivo evaluation of [18F]-FPECMO as a positron emission tomography radioligand for imaging the metabotropic glutamate receptor subtype 5. Nucl Med Biol. 2009;36(6):613–22.
31. Sephton SM, Dennler P, Leutwiler D, Mu L, Wanger-Baumann CA, Schibli R, et al. Synthesis, radiolabelling and in vitro and in vivo evaluation of a novel fluorinated ABP688 derivative or the PET imaging of metabotropic glutamate receptor subtype 5. Am J Nucl Med Mol Imaging. 2012;2(1):14–28.
32. Sephton SM, Mu L, Schweizer WB, Schibli R, Krämer SD, Ametamey SM. Synthesis and evaluation of novel α-fluorinated (E)-3-((6-methylpyridin-2-yl)ethynyl)cyclohex-2-enone-O-methyl oxime (ABP688) derivatives as metabotropic glutamate receptor subtype 5 PET radiotracers. J Med Chem. 2012;55(16):7154–62.
33. Wanger-Baumann CA, Mu L, Honer M, Belli S, Alf MF, Schubiger PA, et al. In vitro and in vivo evaluation of [18F]-FDEGPECO as a PET tracer for imaging the metabotropic glutamate receptor subtype 5 (mGluR5). Neuroimage. 2011;56(3):984–91.
34. Sephton SM, Mu L, Dragic M, Krämer SD, Schibli R, Ametamey SM. Synthesis and in vitro evaluation of E- and Z-geometrical isomers of PSS232 as potential metabotropic glutamate receptor subtype 5 (mGlu5) binders. Synthesis. 2013;45:1877–85.
35. Lavreysen H, Wouters R, Bischoff F, Nobrega Pereira S, Langlois X, Blokland S, et al. JNJ16259685, a highly potent, selective and systemically active mGlu1 antagonist. Neuropharmacology. 2004;47(7):961–72.
36. Elmenhorst D, Aliaga A, Bauer A, Rosa-Neto P. Test-retest stability of cerebral mGluR5 quantification using [11C]ABP688 and positron emission tomography in rats. Synapse. 2012;66(6):552–60.
37. Yu M, Tueckmantel W, Wang X, Zhu A, Kozikowski AP, Brownell AL. Methoxyphenylethynyl, methoxypyridylethynyl and phenylethynyl derivatives of pyridine: synthesis, radiolabeling and evaluation of new PET ligands for metabotropic glutamate subtype 5 receptors. Nucl Med Biol. 2005;32(6):631–40.
38. Anderson JJ, Bradbury MJ, Giracello DR, Chapman DF, Holtz G, Roppe J, et al. In vivo receptor occupancy of mGlu5 receptor antagonists using the novel radioligand [3H]3-methoxy-5-(pyridin-2-ylethynyl)pyridine). Eur J Pharmacol. 2003;473(1):35–40.
39. Kramer SD, Testa B. The biochemistry of drug metabolism – an introduction: Part 6. Inter-individual factors affecting drug metabolism. Chem Biodivers. 2008;5:2465–578.
40. Wang JQ, Tueckmantel W, Zhu A, Pellegrino D, Brownell AL. Synthesis and preliminary biological evaluation of 3-[(18)F]fluoro-5-(2-pyridinylethynyl)benzonitrile as a PET radiotracer for imaging metabotropic glutamate receptor subtype 5. Synapse. 2007;61(12):951–61.